

# Ab initio analysis of some Ge-based 2D nanomaterials

Ali Ghojvand,<sup>1,\*</sup> S. Javad Hashemifar,<sup>1,†</sup> Mahdi Tarighi Ahmadpour,<sup>1</sup>  
Alexander V. Shapeev,<sup>2</sup> Amir Alhaji,<sup>3</sup> and Qaem Hassanzada<sup>1</sup>

<sup>1</sup>*Department of Physics, Isfahan University of Technology, Isfahan, 84156-83111, Iran*

<sup>2</sup>*Skolkovo Institute of Science and Technology, Skolkovo Innovation Center,  
Bolshoy Boulevard 30, bld. 1, Moscow, 121205, Russia*

<sup>3</sup>*Department of Materials Engineering, Isfahan University of Technology, Isfahan 84156-83111, Iran*

(Dated: January 24, 2020)

The structural, electronic and dynamical properties of a group of 2D germanium-based compounds, including GeC, GeN, GeO, GeSi, GeS, GeSe, and germanene, are investigated by employing first-principles calculations. The most stable structure of each of these systems is identified after considering the most probable configurations and performing accurate phonon calculations. We introduce a new phase of germanene, which we name the tile germanene, which is significantly more stable than the known hexagonal germanene. We apply the modern modified Becke-Johnson (mBJ) and DFT1/2 schemes to obtain an accurate band structure for our selected 2D materials. It is seen that GeO and GeC exhibit the highest band gaps of more than 3 eV in this group of materials. Moreover, we argue that, in contrast to the semi-metallic nature of hexagonal germanene, the tile germanene is a very good conductor. The band edges of our semiconducting 2D materials are accurately aligned to the vacuum level to address the potential photocatalytic application of this system for water splitting and carbon dioxide reduction. The optical properties, including dielectric functions, refractive index, reflectivity, and Loss function of the samples are investigated in the framework of the Bethe-Salpeter approach.

## I. INTRODUCTION

In recent years, elemental sheet of germanium, known as germanene, has been emerging as a strong contender in the realm of 2D materials. Germanene is a one-atom-thick germanium layer which has a honeycomb structure (D3d point group) and a zero band gap with a Dirac cone at the K point of the Brillouin zone. In 2009, Cahangirov et al, by using first-principles calculations, predicted a low buckled (corrugated) sheet structure for a 2D germanene layer.<sup>1</sup> The main hurdle experienced in realizing individual germanene layers is that, unlike graphene, they do not form a van der Waals layered structure in their natural form. Hence, top-down approaches are not applicable for synthesis of individual germanene layers. In 2014, the first synthesis of germanene was realized on a gold (111) substrate with a growth mechanism similar to the formation of silicene layers on silver (111) templates.<sup>2</sup>

The absence of band gap dramatically hampers direct applications of germanene in semiconductor devices in nanoelectronics, photoelectronics, and sensors. Hence, seeking an effective method to open a sizable band gap in germanene is an active field of research. Chemical functionalization with small molecules, introducing structural defects, and alloying with proper elements are three conventional methods to engineer the band structure of 2D materials. Hydrogen functionalized germanene layers (GeH) were successfully synthesized in 2013 with a band gap of about 1.5 eV and a similar structure to graphane.<sup>3</sup> Padilha and others considered Stone-Wales (SW), single vacancy, and divacancies defects in germanene and showed that the SW defect open a band gap in the system and destroys the Dirac cone, while the single vacancy defect preserves the Dirac cone.<sup>4</sup> Introducing structural de-

fects such as StoneWales, single vacancy, and divacancies strongly affects the band structure and transport properties of the system, compared with the pristine one. Xu et al. predicted that alloying with Se may lead to the formation of two different semiconducting configurations of GeSe monolayers, which exhibit anisotropic absorption spectra in the visible region.<sup>5</sup>

In this work, we employ first-principles calculations to study the structural, electronic, and optical properties and dynamical stability of a group of Ge-based 2D materials including GeO, GeS, GeSe, GeN, GeC, GeSi, and germanene. In the next section, we introduce the computational techniques used in this work. Then the stability of the systems will be addressed in section III, electronic properties will be explained in section IV, and optical properties will be presented in section V. The summary of our work will be given in the last section.

## II. METHOD

We performed electronic structure calculations and geometry optimization in the framework of density functional theory (DFT)<sup>6,7</sup> and the Perdew, Burke, and Ernzerhof (PBE) exchange-correlation functional<sup>8</sup> by using the full-potential all-electron numeric atom-centered orbital method implemented in the FHI-aims package.<sup>9</sup> In order to obtain very accurate binding energies and optimized geometries, the structure relaxation tolerance was set to 0.001 eV/Å. In order to verify dynamical stability of the structures, phonon calculations were performed by using the density functional perturbation theory and the plane wave ultrasoft pseudopotential method, implemented in the QUANTUM ESPRESSO package.<sup>10</sup> The

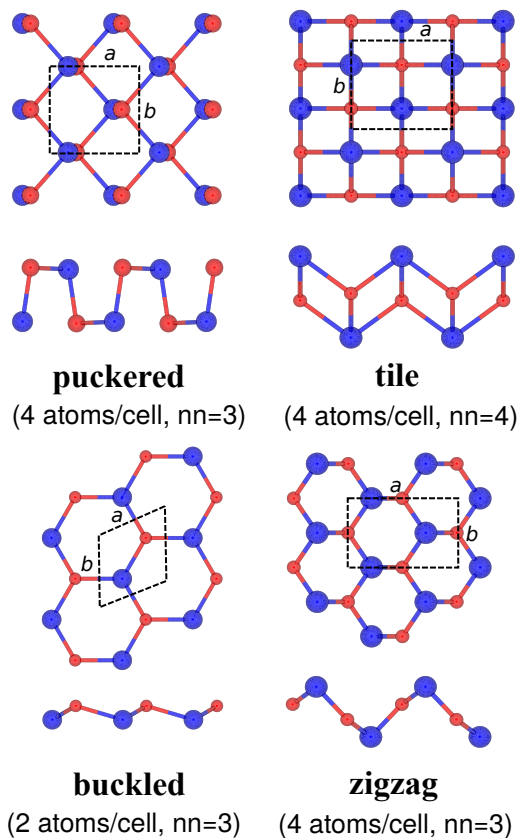


FIG. 1. Top and side views of the four candidate structures for our Ge based 2D materials. The dotted lines encapsulate the 2D unitcell of the lattices and the blue and red balls indicate two nonequivalent atomic positions in the systems.

reliability of the pseudopotentials was verified by comparing the obtained binding energies in the Quantum Espresso and FHI-aims packages. The novel DFT1/2 and modified Becke-Johnson (mBJ) schemes were applied to correct the PBE electronic band structure of the systems. The accuracy of the band gaps in these methods and especially DFT1/2 were comparable with the expensive hybrid functional and GW methods,<sup>11–13</sup> while their required computational effort is comparable to that of PBE. The DFT1/2 method<sup>14</sup>, which extends the Slater's half-occupation technique to bulk materials, were applied by using the Exciting package which employs the full potential linear augmented plane wave method to solve the single particle Kohn-Sham equations.<sup>15</sup> On the other hand, the modified Becke-Johnson (mBJ) method<sup>16</sup> was applied by using the Wien2k package<sup>17</sup> which has a very similar technical structure to the Exciting package. The monolayer structures were simulated in the slab supercells with a vacuum thickness of about 13Å to avoid unrealistic effects from periodic boundary conditions.

The optical properties of the systems were calculated by using the Exciting package which takes into account the nontrivial effects of electron-hole interaction and solves the Bethe-Salpeter equation<sup>18</sup> (BSE):

$$(\varepsilon_{c\mathbf{k}} - \varepsilon_{v\mathbf{k}})A_{c\nu\mathbf{k}}^S + \sum_{\mathbf{k}'c'v'} \kappa_{c'v'\mathbf{k}'}^{c\nu\mathbf{k}} A_{c'v'\mathbf{k}'}^S = \Omega^s A_{c\nu\mathbf{k}}^S$$

where the term  $(\varepsilon_{c\mathbf{k}} - \varepsilon_{v\mathbf{k}})$  refers to the difference between the conduction and valence quasiparticle energies at a specific  $\mathbf{k}$ -point,  $\kappa$  describes the electron-hole interaction, and  $\Omega^s$  is the excitation energy. After solving for the BSE excitation states, the Tomm-Dancoff approximation<sup>19–22</sup> (TDA) is used to compute the imaginary part of the dielectric function ( $\varepsilon_2$ ):

$$\text{Im}(\varepsilon_M^i(\omega)) = \varepsilon_2(\omega) = \frac{16\pi^2 e^2}{\omega^2} \sum_S |\vec{e} \cdot \langle 0 | \vec{v} | S \rangle|^2 \delta(\omega - \Omega^s)$$

where  $\vec{e}$  describes the polarization of the incident light and  $\vec{v}$  is the velocity operator. Then the Kramers-Kronig relations are employed to find the real part of the dielectric function ( $\varepsilon_1$ ) and subsequently other linear optical properties including refractive index  $n(\omega)$ , reflectivity  $R(\omega)$ , and electron loss function  $L(\omega)$ :

$$n(\omega) = \left( \frac{\sqrt{\varepsilon_1^2 + \varepsilon_2^2} + \varepsilon_1}{2} \right)^{1/2}$$

$$k(\omega) = \left( \frac{\sqrt{\varepsilon_1^2 + \varepsilon_2^2} - \varepsilon_1}{2} \right)^{1/2}$$

$$R(\omega) = \frac{(n-1)^2 + k^2}{(n+1)^2 + k^2} \quad L(\omega) = \frac{\varepsilon_2}{\varepsilon_1^2 + \varepsilon_2^2}$$

### III. STABLE STRUCTURES

After a broad literature survey, we realized that the structures of the most novel 2D materials may be generally categorized in the puckered and buckled configurations, presented in Fig. 1, while other structures are rarely investigated in the literature. Hence, we applied these 2D structure patterns to our desired materials; Ge, GeO, GeS, GeSe, GeN, GeC, and GeSi. During geometrical optimizations, in some cases, we noticed appearance of two new structures, called zigzag and tile in Fig. 1, which were added to the candidate structures of our 2D materials. In order to find the most stable structure of each of the systems, we calculated their binding energy in the four candidate structures by comparing the optimized total energies with the energy of corresponding isolated atoms. The obtained binding energies are presented in table I.

It is very interesting to see that these materials mostly admit the buckled configuration as a metastable structure while their lowest-energy structure is among other

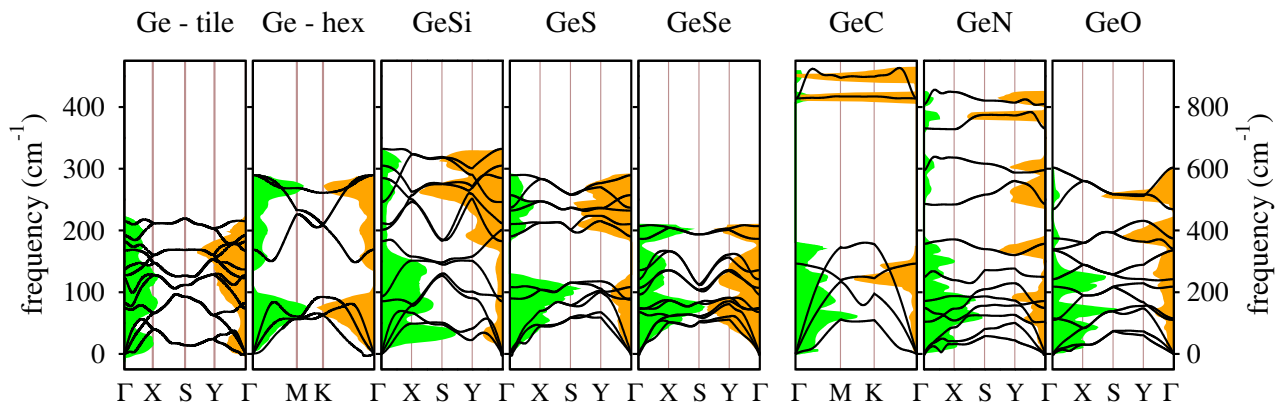


FIG. 2. Obtained phonon band structure of our selected 2D materials. The green and orange shaded areas show the phonon partial density of states of Ge and its partner atoms in our 2D systems, respectively.

TABLE I. Calculated binding energy (eV/atom) and thickness (Å) (in the parenthesis) of the studied 2D materials in the four candidate structures.

	buckled	puckered	zigzag	tile
GeO	-5.60 (0.99)	—	<b>-5.85</b> (2.23)	—
GeS	-4.48 (1.36)	<b>-4.51</b> (2.57)	—	—
GeSe	-4.16 (1.44)	<b>-4.17</b> (2.60)	—	—
GeN	-5.66 (0.00)	—	<b>-6.01</b> (1.26)	—
GeC	<b>-5.98</b> (0.00)	—	—	—
GeSi	-4.34 (0.58)	—	—	<b>-4.52</b> (1.95)
Ge	-4.01 (0.67)	—	—	<b>-4.12</b> (1.97)

TABLE II. Relaxed structural parameters  $a, b$  and average nearest neighbor bond lengths  $d1$  and  $d2$  (Å) of the investigated 2D systems, in their most stable structure.

	GeO	GeS	GeSe	GeN	GeC	GeSi	Ge-tile
$a$	4.64	4.54	4.29	5.36	3.23	3.94	4.19
$b$	3.01	3.63	3.98	3.06	3.23	3.64	3.83
$d1$	1.97	2.43	2.54	2.17	1.87	2.69	2.71
$d2$	1.97	2.46	2.66	1.96	1.87	2.58	2.71

candidates. It is more fascinating in the case of germanene, where its well known hexagonal structure (zero buckled) is considerably less stable than our discovered tile structure. A more reliable and detailed investigation of this issue requires studying dynamical stability which will be presented later. The obtained results indicate that the binding energy is decreasing with the increase of the atomic radius. In other words, oxygen, nitrogen, and carbon atoms which are the smallest atoms in our samples give rise to the highest binding energies for the GeO, GeN, and GeC compounds. On the other hand, Ge which has the largest atomic radius leads to the lowest binding energy for the 2D germanene. This trend indicates a stronger bonding between atoms with smaller radii which is in agreement with the physical intuition. The equilibrium lattice constants and bond lengths of the lowest-energy structures of GeO, GeS, GeSe, GeN,

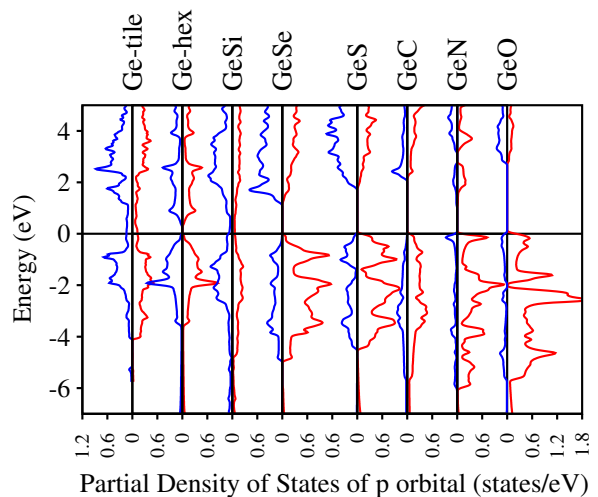


FIG. 3. Contribution of p orbitals of Ge (blue, left oriented) and its partner atom (red, right oriented) in the density of states of the investigated 2D systems.

GeC, GeSi, and germanene are calculated and presented in Table II.

As it was mentioned before, phonon calculations should be done to confirm the stability of the lowest-energy structures. The phonon dispersion curves of all the materials at their lowest-energy structure were computed by using the density functional perturbation theory method. The obtained phonon spectra of the samples along their high symmetry paths in the reciprocal space are presented in Fig. 2. The absence of any negative (imaginary) frequency mode in the spectra demonstrates dynamical stability of all the systems. We observe that GeC, GeN, and GeO display the widest range of phonon modes among the studied systems, providing further evidence for stronger bonding in these systems, compared with others. Especially in GeC, a large distance seen between the acoustic modes and the two optical modes which is an evidence of a strong directional bonding in

this system. In the new phase of germanene, in contrast to the hexagonal phase, we observe that the optical modes are not well separated from the acoustic modes, which may be attributed to the softer bonding in the tile germanene.

For better understanding of the dynamical features of the systems, we calculated the phonon partial density of states (PDOS) of Ge and its partner atoms in our investigated 2D materials. The results are presented as shaded areas in Fig. 2. It is clearly seen that the heavy elements Ge and Se have a larger contribution to the acoustic phonon modes while the light elements exhibit stronger vibrations in the optical modes.

Dynamical stability of the new phase of germanene along with its lower binding energy, compared with the hexagonal germanene, raises the question of why this phase has not yet been observed in real samples. In order to address this question one should note that within all successful synthesis of germanene, the [111] surface of gold or platinum has been used as the substrate. These surfaces involve hexagonal arrangement of the substrate atoms which may enhance formation of hexagonal germanene on the surface. Hence, atomistic growth of germanene atoms on square-symmetry surfaces may enhance the formation of tile germanene in realistic samples.

#### IV. ELECTRONIC STRUCTURE

The obtained electronic PDOS of the systems in their lowest-energy structure, within PBE, are presented in Fig. 3. It is seen that the systems with the highest binding energies (GeO, GeN, and GeC) exhibit the most broadened valence bands, in agreement with strong bonding in these systems. Moreover, the valence p orbital of Ge in GeO and GeN is effectively evacuated and transferred to the valence p orbital of its partner atom, indicating significant ionic bonding in these two monolayers. GeSi and the two configurations of germanene represent a metallic electronic structure while the other investigated 2D materials are semiconductors. The tile configuration of germanene is likely a very good conductor, because it has a finite density of high mobility p electrons at the Fermi level.

In order to obtain more accurate electronic structures, as it was mentioned in the Methods, we apply the DFT1/2 and mBJ schemes which have been proven to predict much more accurate band gaps, compared with the conventional LDA and GGA functionals. The calculated electronic band structures of GeO, GeS, GeSe, GeN, GeC and GeSi within the DFT1/2 and mBJ schemes along the high-symmetry directions of the Brillouin zone are presented in Fig. 4. It is seen that these two methods predict quite similar band structures, except for the position of Fermi levels which are occasionally different. More discussion on the relative positions of Fermi levels and band edges needs to the alignment of the energy references which will be presented in the next paragraphs.

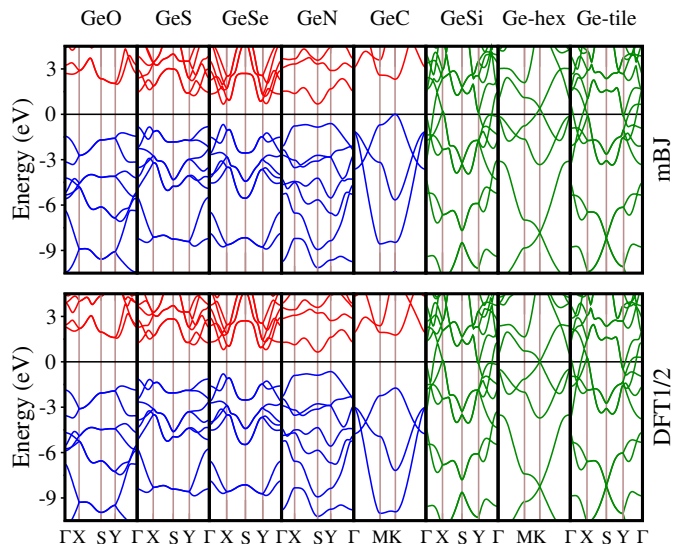


FIG. 4. Electronic band structures of our Ge based 2D compounds within the mBJ (top row) and DFT1/2 (bottom row) methods.

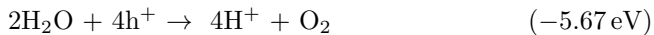
Among the studied systems, GeC exhibit the most peculiar band structure with very high valence band dispersion, indicating a very stiff directional bonding in this system. This observation is consistent with the large distance observed between the acoustic and optical phonon modes of this system (Fig. 2). We observe that the Dirac cone of hexagonal germanene is slightly shifted within mBJ, indicating less accuracy of the mBJ Fermi level, compared with DFT1/2. GeSi and tile germanene exhibit similar band structures, because both systems stabilize in the tile structure and have similar atomic valence shell. The same similarity is visible between GeS and GeSe band structures. The calculated values for the energy gaps are summarized in Table III. In this table the reported band gap within the hybrid HSE06 functionals<sup>23,24</sup> are also given for comparison. We observe that the predicted band gaps within DFT1/2 are closer to the HSE06 gaps, compared with the mBJ functional. Due to the lack of experimental data, we are not able to compare the accuracy of the DFT1/2 and HSE06 methods, although in the case of bulk semiconductors there is some evidences for a higher accuracy of the DFT1/2 scheme.<sup>25</sup>

2D materials are generally considered as potential candidates for photocatalytic applications in various chemical reactions. Because in these nanomaterials, the relative surface area is very large, the transport distance for the photo generated carriers to reach the reaction interface is very short, and the band gap is likely enlarged due to the quantum confinement effect<sup>29</sup>. Therefore, we screen the band edges of our germanium-based 2D materials to investigate their potential photocatalytic application in the water splitting and carbon dioxide conversion

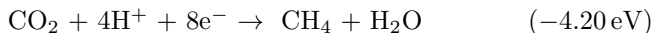
TABLE III. Calculated band gap (eV) of GeS, GeSe, GeC, GeO, and GeN in their most stable structures within the PBE, DFT1/2 and mBJ methods. The most accurate reported band gaps within HSE06 and GW0 scheme are also given in the last column as the best theoretical references.

	PBE	DFT1/2	mBJ	others
GeO	2.84	3.22	3.27	3.73 [HSE] <sup>26</sup>
GeS	1.79	2.27	2.06	2.32 [HSE] <sup>27</sup>
GeSe	1.22	1.68	1.41	1.61 [HSE] <sup>5</sup>
GeN	1.05	1.29	1.30	—
GeC	2.06	3.50	2.32	3.56 [GW] <sup>28</sup>

reactions. The water splitting reactions are:



where  $\text{h}^+$  and  $\text{e}^-$  are the photo-generated hole and electron and numbers in the parenthesis are the corresponding redox potentials at room temperature and zero pH<sup>30</sup>. A proper photocatalyst for these reactions should have a conduction band bottom (CBB) below the hydrogen evolution potential and a valence band top (VBT) above the oxygen evolution potential. In addition to the above water splitting reactions, we considered carbon dioxide conversion to methanol, formic acid, and methane as follows:



As it was mentioned before, the numbers in the parenthesis are corresponding reduction potentials at room temperature and zero pH<sup>31</sup>. In order to consider other temperature and pH values, the redox potentials should be shifted by  $\text{pH} \times (\text{K}_B \text{T} \times \ln 10)$ . The CBB of the proper semiconductor photocatalyst for the above mentioned conversions should be above the corresponding reduction potentials.

The band edges of our 2D systems were determined with respect to the vacuum level potential within the DFT1/2 and mBJ schemes and the resulting CBBs, VBTs, and Fermi levels are compared with the above mentioned redox potentials in Fig. 5. The vacuum level is determined by averaging the electrostatic potential of the slab supercells in the horizontal planes and then plotting the averaged potential as a function of vertical position  $z$ . The obtained CBB band edges clearly indicate that all our five 2D semiconductors (GeO, GeS, GeSe, GeN, and GeC) are good photocatalyst candidates for the three considered carbon dioxide reduction reactions and the  $\text{H}^+/\text{H}_2$  water splitting half-reaction. On the other hand, GeO, GeS, and GeC may be good photocatalysts for the  $\text{H}_2\text{O}/\text{O}_2$  water splitting half-reaction while GeSe needs a rather little bias of less than 0.2 eV to photocatalyse this reaction.

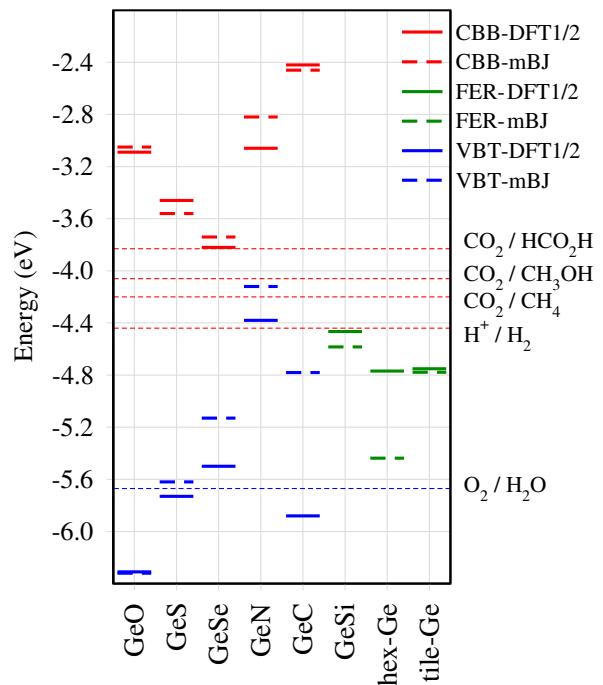


FIG. 5. Valence band top (VBT), conduction band bottom (CBB), and Fermi (FER) levels of the studied 2D systems with respect to the vacuum level within DFT1/2 and mBJ schemes.

## V. OPTICAL PROPERTIES

As it was mentioned in the section Method, we investigated the optical properties of our 2D materials in the framework of the Bethe-Salpeter approach. The obtained optical properties including the real and imaginary parts of the dielectric function, reflectivity, refraction index, and the energy loss function are presented in Fig. 6. Optical properties are calculated for two polarization of the incident light electric field along the  $x$  and  $y$  directions. Comparing the  $xx$  and  $yy$  components of optical parameters indicate that GeC and hexagonal germanene are well isotropic in the  $xy$  plane in whole frequency range, while other 2D systems exhibit clear in-plane anisotropies in the frequencies below 10 eV, being attributed to the anisotropic crystal structure of these materials. The observed in-plane anisotropy is more pronounced in GeO, GeS, and tile germanene. It is interesting to see that the new invented structure of germanene exhibit strong anisotropy in all optical parameters in low frequencies, below 2 eV. The strong anisotropy of the refractive index will likely lead to birefringence behavior of tile germanene in low frequencies. The results show high reflectivity of GeS, GeSe, GeSi, and hexagonal germanene in a broad frequency range. On the other hand, GeS, GeSe, and GeSi exhibit very low refractive index around frequency of 8 eV, in the UV region.

The first peak in the imaginary part of the dielectric function is expected to give the optical gap of semicon-

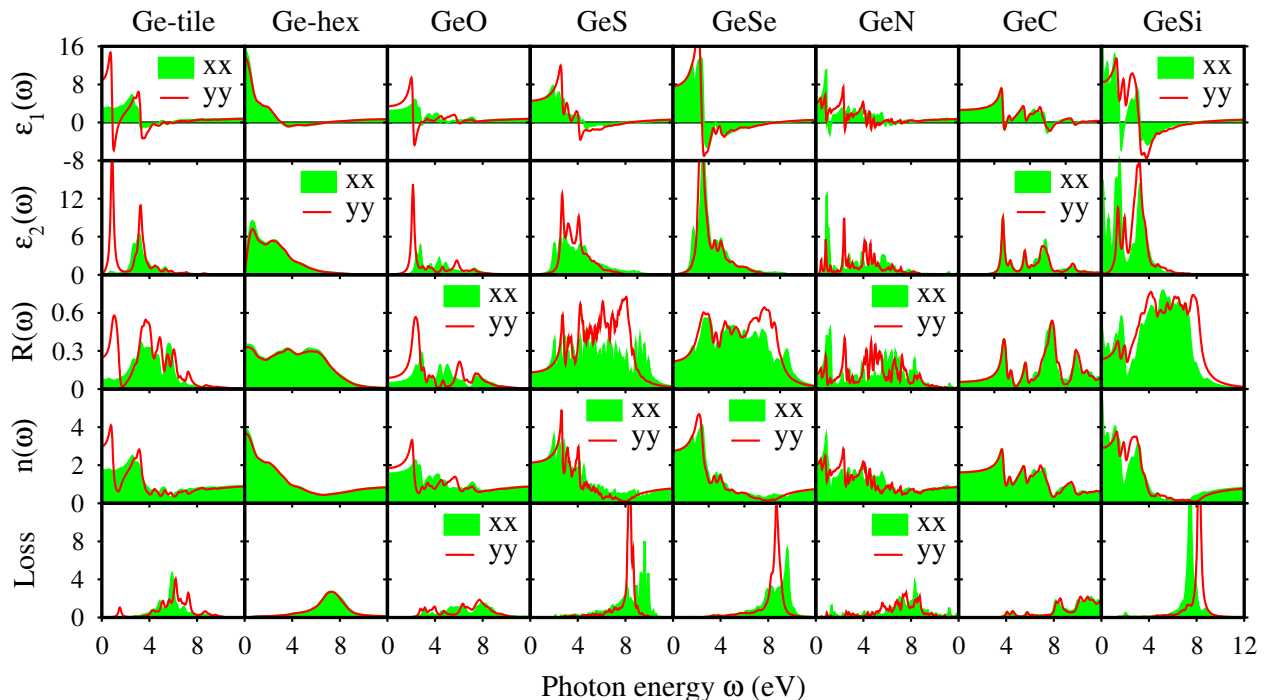


FIG. 6. Optical properties of our investigated 2D materials, including the real ( $\epsilon_1(\omega)$ ) and imaginary ( $\epsilon_2(\omega)$ ) parts of the dielectric function, reflectivity ( $R(\omega)$ ), refractive index  $n(\omega)$ , and energy loss function, calculated for the x (green shaded area) and y (red solid line) polarizations of the incident light.

ductors, while the characteristic frequency of metals, corresponding to the collective excitations of valence electrons, known as plasma frequency, is given by those peaks of the loss function which are located around nodes of the real part of the dielectric function. The optical gap and plasma frequencies of the systems were determined and presented in table IV. The corresponding zero energy value of the real part of dielectric function, known as static relative permittivity, is also extracted and given in this table. It is seen that GeSi and hexagonal germanene shows the highest static relative permittivity among our studied systems. The largest optical gap is observed in GeC, while GeN has a small optical gap of about 0.45 eV. Since the calculated optical responses are obtained in the presence of the attractive electron-hole interaction (excitonic effects), well described in the Bethe-Salpeter approach, the distance between the optical gap and the electric gap is introduced as a measure of the exciton binding energy of the system.<sup>18,32</sup> In the framework of electronic structure theory, the electric gap is determined by the many body based GW scheme and as it was mentioned before, the GW gaps are expected to be very close to the obtained gaps within the DFT1/2 scheme<sup>25</sup> (table III). Hence, we calculated the exciton binding energy of our 2D systems as the difference between their optical and DFT1/2 gaps and presented the results in table IV. We observe a very low exciton binding energy for GeC and GeSe, which may indicate a very low carrier recombination rate in these systems after photo-excitations. This

TABLE IV. Obtained static value (at  $\omega = 0$ ) of the real part of dielectric function, optical gap (eV), exciton binding energy  $\Delta_X$  (eV), and plasma frequencies  $\omega_p$  (eV) of the investigated 2D systems.

	$\epsilon_{xx}^1$	$\epsilon_{yy}^1$	gap	$\Delta_X$	$\omega_p$
GeO	2.42	3.33	2.15	1.07	2.85
GeS	4.33	4.56	2.04	0.23	8.32
GeSe	7.21	7.62	1.68	0.00	8.56
GeN	4.61	4.09	0.45	0.84	1.33, 2.55
GeC	2.63	2.63	3.50	0.00	4.05, 8.45
GeSi	12.94	8.59	—	—	2.02, 8.14
Ge-tile	2.93	8.70	—	—	1.48, 4.88
Ge-hex	14.84	13.49	—	—	—

observation encourages photocatalytic and photovoltaic applications of 2D GeC and GeSe materials.

The last column in table IV shows the predicted plasma frequencies of our systems. Although, plasma frequency is usually a characteristic feature of metallic systems, as it is seen in the case of our 2D semiconductors, semiconducting materials may also exhibit this kind of collective excitation of valence electrons.<sup>33</sup> While most of the investigated 2D systems has a plasma frequency in the UV region, we observe that plasma oscillations in the visible region may happen in the semiconducting GeO and GeN and metallic GeSi 2D materials. The results show that, in the IR region, only metallic tile germanene and semiconducting GeN may exhibit plasmonic excita-

tions.

## VI. CONCLUSIONS

In summary, we carried out a comprehensive first-principles study to investigate electronic and optical properties of eight Ge based 2D materials. The calculated binding energies and phonon spectra indicate that GeO and GeN monolayers stabilize in a zigzag structure, GeS and GeSe sheets prefer a puckered configuration, and GeC occurs in a zero buckled (honeycomb) lattice. In the case of germanene monolayer, we obtained a new structure, called as tile germanene, which is about 0.11 eV/atom more stable than the known hexagonal structure of germanene. The obtained electronic structures suggest that tile germanene and GeSi are very good semiconductors, while GeO, GeN, GeS, GeSe, and GeC display a band gap in their electronic structure. The novel DFT1/2 scheme was applied to obtain reliable and accurate band gaps. The largest band gap is

seen in GeC (3.50 eV) while GeN exhibits the smallest band gap (1.29 eV) among these systems. We used the vacuum level potential in the slab supercell as the energy reference to determine the absolute band edges of the semiconducting systems. The resulting valence and conduction band edges suggest potential application of the GeO, GeS, and GeC monolayers as photocatalyst for water splitting. The Bethe-Salpeter approach was used to compute various optical properties, optical band gap, and plasma frequencies of the samples in the presence of excitonic effects. We observed a very low exciton binding energy in the GeC and GeSe sheets which further encourage photocatalytic application of these 2D materials.

## VII. ACKNOWLEDGMENTS

This work was supported by the Vice Chancellor of Isfahan University of Technology (IUT) in Research Affairs.

- 
- \* a.ghojavand@ph.iut.ac.ir  
 † hashemifar@iut.ac.ir
- <sup>1</sup> S. Cahangirov, M. Topsakal, E. Aktürk, H. Şahin, and S. Ciraci, *Physical review letters* **102**, 236804 (2009).
  - <sup>2</sup> M. Davila, L. Xian, S. Cahangirov, A. Rubio, and G. Le Lay, *New J. Phys* **16**, 095002 (2014).
  - <sup>3</sup> E. Bianco, S. Butler, S. Jiang, O. D. Restrepo, W. Windl, and J. E. Goldberger, *Acs Nano* **7**, 4414 (2013).
  - <sup>4</sup> J. E. Padilha and R. B. Pontes, *Solid State Communications* **225**, 38 (2016).
  - <sup>5</sup> Y. Xu, H. Zhang, H. Shao, G. Ni, J. Li, H. Lu, R. Zhang, B. Peng, Y. Zhu, H. Zhu, *et al.*, *Physical Review B* **96**, 245421 (2017).
  - <sup>6</sup> P. Hohenberg and W. Kohn, *Physical review* **136**, B864 (1964).
  - <sup>7</sup> W. Kohn and L. Sham, *Phys. Rev. A* **140**, 113 (1965).
  - <sup>8</sup> J. Perdew, K. Burke, and M. Ernzerhof, *Errata:(1997) Phys Rev Lett* **78**, 1396 (1996).
  - <sup>9</sup> V. Blum, R. Gehrke, F. Hanke, P. Havu, V. Havu, X. Ren, K. Reuter, and M. Scheffler, *Computer Physics Communications* **180**, 2175 (2009).
  - <sup>10</sup> P. Giannozzi, S. Baroni, N. Bonini, M. Calandra, R. Car, C. Cavazzoni, D. Ceresoli, G. L. Chiarotti, M. Cococcioni, I. Dabo, *et al.*, *Journal of physics: Condensed matter* **21**, 395502 (2009).
  - <sup>11</sup> L. Hedin, *Physical Review* **139**, A796 (1965).
  - <sup>12</sup> R. W. Godby and R. Needs, *Physical review letters* **62**, 1169 (1989).
  - <sup>13</sup> M. S. Hybertsen and S. G. Louie, *Physical Review B* **34**, 5390 (1986).
  - <sup>14</sup> L. G. Ferreira, M. Marques, and L. K. Teles, *Physical Review B* **78**, 125116 (2008).
  - <sup>15</sup> A. Gulans, S. Kontur, C. Meisenbichler, D. Nabok, P. Pavone, S. Rigamonti, S. Sagmeister, U. Werner, and C. Draxl, *Journal of Physics: Condensed Matter* **26**, 363202 (2014).
  - <sup>16</sup> F. Tran and P. Blaha, *Physical review letters* **102**, 226401 (2009).
  - <sup>17</sup> K. Schwarz, P. Blaha, and S. Trickey, *Molecular Physics* **108**, 3147 (2010).
  - <sup>18</sup> G. Onida, L. Reining, and A. Rubio, *Reviews of modern physics* **74**, 601 (2002).
  - <sup>19</sup> M. Rohlfing and S. G. Louie, *Physical Review B* **62**, 4927 (2000).
  - <sup>20</sup> L. X. Benedict, E. L. Shirley, and R. B. Bohn, *Physical review letters* **80**, 4514 (1998).
  - <sup>21</sup> J.-W. Van der Horst, P. Bobbert, M. Michels, G. Brocks, and P. Kelly, *Physical review letters* **83**, 4413 (1999).
  - <sup>22</sup> A. L. Fetter and J. D. Walecka, *Quantum theory of many-particle systems* (Courier Corporation, 2012) pp. 538–539.
  - <sup>23</sup> J. Heyd, G. E. Scuseria, and M. Ernzerhof, *The Journal of chemical physics* **118**, 8207 (2003).
  - <sup>24</sup> H. J. S. GE and M. Ernzerhof, *J. Chem. Phys* **124**, 219906 (2006).
  - <sup>25</sup> J. Doumont, F. Tran, and P. Blaha, *Physical Review B* **99**, 115101 (2019).
  - <sup>26</sup> Y. Guo, L. Ma, K. Mao, M. Ju, Y. Bai, J. Zhao, and X. C. Zeng, *Nanoscale Horizons* **4**, 592 (2019).
  - <sup>27</sup> L. C. Gomes and A. Carvalho, *Physical Review B* **92**, 085406 (2015).
  - <sup>28</sup> H. Şahin, S. Cahangirov, M. Topsakal, E. Bekaroglu, E. Akturk, R. T. Senger, and S. Ciraci, *Physical Review B* **80**, 155453 (2009).
  - <sup>29</sup> S. Hu and M. Zhu, *ChemCatChem* (2019).
  - <sup>30</sup> S. Trasatti, *Pure and Applied Chemistry* **58**, 955 (1986).
  - <sup>31</sup> D. K. Kanan and E. A. Carter, *The Journal of Physical Chemistry C* **116**, 9876 (2012).
  - <sup>32</sup> Z.-h. Yang and C. A. Ullrich, *Physical Review B* **87**, 195204 (2013).
  - <sup>33</sup> P. Y. Yu and M. Cardona, *Fundamentals of semiconductors: physics and materials properties* (Springer, 1996) p. 427.